Mon. Not. R. Astron. Soc. **000**, 1–12 (2007) Printed 1 February 2008 (MN LATEX style file v2.2)

The dust temperatures of the prestellar cores in the ρ Oph main cloud and in other star forming regions: consequences for the core mass function

Dimitris Stamatellos⋆, Anthony P. Whitworth, and Derek Ward-Thompson
School of Physics & Astronomy,Cardiff University, Cardiff, CF24 3AA, Wales, UK

Accepted 1988 December 15. Received 1988 December 14; in original form 1988 October 11

ABSTRACT

We estimate the dust temperatures of the clumps in the ρ Oph main cloud taking into account the 3D geometry of the region, and external heating from the interstellar radiation field and from HD147879, a nearby luminous B2V star, which is believed to dominate the radiation field in the region. We find that the regions where prestellar cores are observed (i.e. at optical visual extinctions > 7 mag) are colder than $\sim 10-11$ K. These dust temperatures are smaller than those which previous studies of the same region have assumed. We use the new dust temperatures to estimate the masses of the prestellar cores in the ρ Oph main cloud from mm observations, and we find core masses that are larger than previous estimates by a factor of $\sim 2-3$. This affects the core mass function (CMF) of the region; we find that the mass at which the core mass spectrum steepens from a slope $\alpha \sim 1.5$ to a slope $\alpha \sim 2.5$ has moved from ~ 0.5 M$_\odot$ to ~ 1 M$_\odot$. In contrast with the CMF in other star forming regions (e.g. Orion), there is no indication for a turnover down to the completeness limit (~ 0.2 M$_\odot$), but the CMF may flatten at around ~ 0.4 M$_\odot$.

We generalize our results to the prestellar cores in Taurus and in Orion. In Taurus the ambient radiation field heating the prestellar cores is believed to be weaker than than that in ρ Oph. Hence, the dust temperatures of the cores in Taurus are expected to be below $\sim 10-11$ K. In Orion the radiation field is believed to be 10^3 times stronger than the standard interstellar radiation field. Based on this assumption we estimate that the dust temperatures of the prestellar cores in Orion are around $\sim 20-30$ K.

Key words: Stars: formation – ISM: clouds-structure-dust – Methods: numerical – Radiative transfer

1 INTRODUCTION

Prestellar cores are condensations in molecular clouds that are on the verge of collapse or already collapsing (e.g. Myers & Benson 1983; Ward-Thompson et al. 1994, 1999; Ward-Thompson, André & Kirk 2002). They represent the first phase in an evolutionary model of star formation that is based on observations of different types of young objects: starless core/prestellar core → Class 0 → Class I → Class II → Class III (Lada 1987; André et al. 1993; André et al. 2000; Di Francesco et al. 2007; Ward-Thompson et al. 2007). The study of starless/prestellar cores is important in constraining the initial conditions for star formation. Prestellar cores have been observed both in groups (as in e.g Ophiuchus, Taurus, Perseus) and in relative isolation (e.g. B68; Alves et al. 2001). They are very cold; their temperatures are below 20 K and most probably around 10 K (Evans et al. 2001; Stamatellos & Whitworth 2003a,b; Stamatellos et al. 2004). They are also very dense; their typical central densities are $\gtrsim 10^5 \mathrm{cm}^{-3}$. They are observed either at NIR wavelengths where they are seen in absorption against the luminous background (e.g. Bacmann et al. 2000), or at FIR and submm wavelengths, where they appear in emission (e.g. Motte et al. 1998; Ward-Thompson et al. 2002; Kirk et al. 2005). The peak of their emission is around 150-200 μm, consistent with the fact that they are very cold.

Submm and mm observations are often used to determine the masses of cores (e.g. Motte et al. 1998; Nutter et al. 2007). At these wavelengths the core is optically thin to the radiation it emits, hence the observed flux from the core is $F_\lambda = \tau_\lambda \; B_\lambda(T_{\rm dust})$. Therefore the column density $N(H_2)$ along the line of sight is

$$N(H_2) = \frac{F_\lambda}{\mu m_H \; \Delta\Omega \; \kappa_\lambda \; B_\lambda(T_{\rm dust})} \; , \qquad (1)$$

⋆ E-mail:D.Stamatellos@astro.cf.ac.uk

where $\Delta\Omega$ is the solid angle of the telescope beam for a resolved source, or the solid angle of the source if unresolved, $N(H_2)$ is the hydrogen column density, κ_λ is the dust opacity per unit mass, and $T_{\rm dust}$ the temperature of the dust (Hildebrand 1983). The above relation assumes that the dust is isothermal along the line of sight within the core. The mass of the core is then determined from the column density, $M_{\rm core} = \int N(H_2) dS$, where the integral is over the projected area of the core. The main uncertainties in determining core masses using the above method come from our limited knowledge of the properties of the dust in cores (κ_λ) and the dust temperature ($T_{\rm dust}$). Eq. 1 is very sensitive to the temperature, since at these low temperatures the Planck function is non-linear and the Rayleigh-Jeans approximation is not valid. Hence, even underestimating or overestimating the core temperature by a few degrees may lead one to overestimate or underestimate the Planck function (and consequently the core mass) by a factor of 2 to 3 (Stamatellos & Whitworth 2005b).

It is important then to investigate whether the core temperatures estimated by previous authors using the core SED (defined by observations at only a few wavelengths) are actually representative of the dust temperatures in cores. The aim of this paper is to use detailed 3D radiative transfer modelling, taking into account the core environment (e.g. nearby luminous sources, ambient cloud), to estimate the temperatures in prestellar cores. We will focus our study on the cores in the ρ Oph main cloud, but we will attempt to generalise our results to other star forming regions.

2 THE ρ OPH MAIN CLOUD

ρ Ophiuchi is a star forming region where many prestellar cores have been observed (see Motte et al. 1998; Nutter et al. 2006) along with more evolved protostars (Class 0, I, II objects; e.g. Motte et al. 1998; Bontemps et al. 2001; Wilking et al. 1989; André & Montmerle 1994). It is one of the closest star-forming regions, being at a distance from 140 to 160 pc (Bontemps et al. 2001; Motte et al. 1998).

We shall confine our study to the ρ Oph main cloud (i.e. L1688), where six major clumps[1] have been identified (Oph-A, Oph-B, Oph-C ,Oph-D, Oph-E and Oph-F). The prototypical Class 0 object VLA1623 (André et al. 1993) is located in the Oph-A clump. Each of these clumps contains a few tens of solar masses and has an extent of ~ 0.3 pc. These clumps show substructure; a large number ($\gtrsim 60$) prestellar cores have been identified in them. The core mass function in the ρ Oph main cloud is similar to the stellar IMF, which suggests that the masses of stars are determined by fragmentation at a very early stage (Motte et al. 1998).

The external radiation field incident on these clumps is believed to be dominated by HD147889, a nearby B2V star, which is located at a distance $0.5-1$ pc away from from the far side of the Oph-A clump (Liseau et al. 1999). This is a luminous star of 5500 $L_\odot$ (Wilking et al. 1989). Assuming a distance of 1 pc and a clump radius of 0.2 pc, if there is no attenuation, 1% of the star's radiation will heat the clump, i.e. 55 $L_\odot$. This radiation dwarfs any radiation from other sources (e.g. the interstellar radiation field, nearby young protostars).

Observations of the wider area of the main ρ Oph cloud (~ 4 deg^2) using SCUBA on the JCMT and comparison with 2MASS extinction maps as part of the COMPLETE project (Ridge et al. 2006) reveal that there are no prestellar cores (at least down to the SCUBA detection limit) at visual extinctions $< 7-10$ mag (Johnstone et al. 2004). It is presumed that the UV radiation present in regions of low visual extinction makes these regions hostile for star formation (McKee 1989). Surveys in other star forming regions have also revealed similar extinction thresholds that appear to be connected to the environment of the region (e.g. in Perseus the extinction threshold is lower, $A_{\rm V} > 5-7$ mag; Kirk et al. 2006).

Thus, it appears that most cores are quite embedded in their parent molecular clouds. Previous radiative transfer simulations of embedded cores suggest that such cores are very cold (Stamatellos & Whitworth 2003a,b; Stamatellos et al. 2004). The temperatures at their centres is around 6 K and at their edges is from around 11 K (for a core embedded in a parent cloud of $A_{\rm V} = 5$) to 9 K (for a core embedded in a parent cloud of $A_{\rm V} = 20$). This is because the deeper the core is embedded the lower is the strength of the radiation field that heats the core. Hence, it is appropriate to ask whether previous studies of prestellar cores have assumed core temperatures that are consistent with the fact that these cores are deeply embedded in their parental clouds.

We focus our study initially on the ρ Oph region. Our goal is to construct a radiative transfer model to estimate the temperature of the cores in this region taking into account the 3D geometry of the region and the role of HD147879 in externally heating the clumps. We will discuss the applicability of this study to other regions of star formation where low-mass stars form, and to more energetic regions of star formation, such as the Orion nebula, by discussing the role of a stronger external radiation field.

The structure of the paper is as follows. In Section 3 we discuss the radiative transfer method we use and the constituents of the model (i.e. radiation sources, model geometry, dust properties, clump density profile). In Section 4 we describe the results of the radiative transfer modelling with respect to the temperature profile and the SEDs of the clumps in ρ Oph, and in Section 5 we discuss the implication of the estimated dust temperature for the core mass function of ρ Oph. In Section 6, we discuss the dust temperatures of cores in other star forming regions, and finally in Section 7 we summarize our results.

3 THE MODEL

The big clumps of ρ Oph are represented by Plummer-like density profiles, i.e. we invoke a spherical geometry, with the density being approximately flat in the centres of clumps and dropping as r^{-2} in the envelopes. We exclude the Oph-B1 clump, which is quite flattened, and the Oph-E clump, which appears to be part of Oph-C. We shall assume that the cores in the clumps are superimposed on this density profile,

[1] To avoid confusion we note that we use the term *clump* to refer to the larger structures and the term *core* to refer to the condensations, i.e. the substructure, in these clumps. Some authors (e.g. Motte et al. 1998) use the reverse terminology.

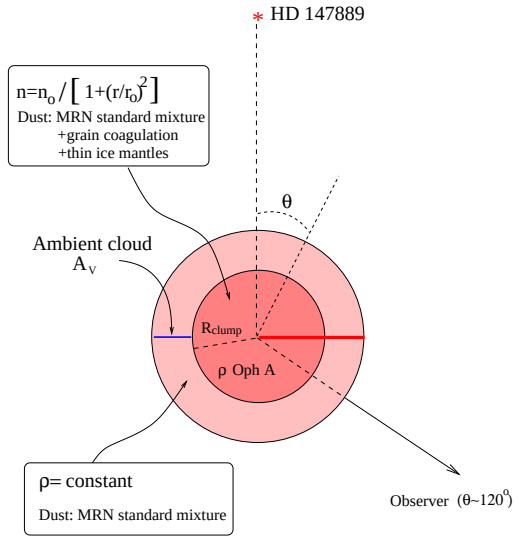

Figure 1. Schematic representation of the ρ Oph A model. The ρ Oph A clump is surrounded by a virtual ambient cloud that modulates the incident radiation that heats the clump. The external heating is provided both by the interstellar radiation field and by HD147889, a nearby B2V luminous star. The general geometry of the models for the other ρ Oph clumps are similar to this one.

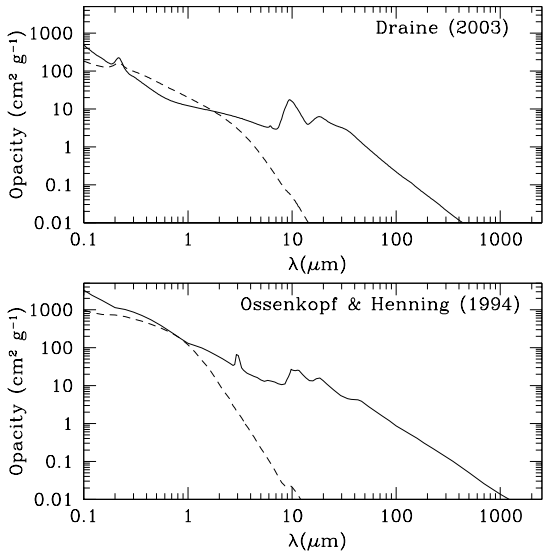

Figure 2. Dust opacity for the clumps (Ossenkopf & Henning 1994) and the virtual ambient cloud (Draine 2003). The solid lines correspond to the opacity due to absorption, and the dashed lines to the opacity due to scattering.

without actually taking them individually into account in this model. However, in Section 4.7 we shall estimate their effect on the dust temperatures. We also assume that these clumps are heated (i) by the interstellar radiation field and (ii) by radiation from the HD14789 B2V star (see Fig.1). We will adopt the 3D model constructed by Liseau et al. (1999). Hence, in our model these clumps define the optical depth that the external radiation has to penetrate to reach the individual cores embedded inside the clumps. In the next subsections we describe in detail the model.

3.1 Density profiles

Each of the ρ Oph clumps is represented by a density profile,

$$n(r) = n_0 \frac{1}{1 + \left(\frac{r}{r_0}\right)^2}, \quad (2)$$

where n_0 is the density at the centre of the clump, and r_0 is the extent of the region in which the density is approximately uniform. This profile is approximately flat in the central region and falls of as r^{-2} in the envelope, similarly to the more commonly used Bonnor-Ebert sphere density profile (Ebert 1955; Bonnor 1956). Additionally, despite being ad hoc, it fits well the observed profiles of prestellar cores and it predicts lifetimes, accretion rates, collapse velocity fields, SEDs and isophotal maps which agree well with observation, using a minimum number of free parameters (Whitworth & Ward-Thompson 2001). The adopted values for n_0, r_0 and the extent $R_{\rm clump}$ of each clump are listed in Table 1. These values are consistent with observations of these clumps (e.g. Motte et al. 1998; André et al. 1993). We assume that the cores in the clumps are superimposed on this density profile (we re-iterate that at this stage we ignore the sub-structure of the clump).

Each clump is surrounded by a virtual ambient cloud, which has a uniform density. The role of these ambient clouds is to modify the ambient radiation field that heats each clump externally. The optical extinction through the ambient cloud is chosen so that the peak of computed SED of each clump corresponds to a dust temperature that matches the dust temperature of each clump assumed by previous authors. The optical extinctions of the assumed ambient clouds around each one of the ρ Oph clumps are also listed in Table 1.

3.2 Dust properties

We use two kinds of dust; one for the clumps, and one for the ambient cloud (Fig. 2). The dust grains in dense clumps are expected to coagulate and accrete ice mantles, so we use the Ossenkopf & Henning (1994) opacities for MRN dust that has coagulated and accreted thin ice mantles for a period of 10^5 years at a density 10^6 cm^{-3}. The ambient cloud has relatively low density and it can be considered as a part of the interstellar medium. Hence, for this layer a standard MRN dust opacity is used (Draine 2003).

3.3 Radiation sources & geometry of the model

Each clump is heated (i) by the interstellar radiation field, attenuated through the ambient cloud, and (ii) by HD147889, a B2V nearby star which is located at distance $\sim 0.5-1$ pc from the ρ Oph region (e.g. Liseau et al. 1999). In this model we will ignore radiation from deeply embedded protostars in these clumps (e.g. VLA 1623, IRS43). According to the Stamatellos et al. (2005) model the presence of an embedded protostar heats only the region around it, hence the results presented here are not greatly affected by the presence of young protostars in or around the clumps. In Section 4.6 we shall discuss the effects of such embedded protostars.

Table 1. (I) Assumed parameters for each clump (based on observations). (II) Results of the radiative transfer modelling.

	Parameter	ρ Oph A	ρ Oph B-2	ρ Oph C	ρ Oph D	ρ Oph F
(I)	$R_{\rm clump}$ [a] (AU)	2×10^4	2.9×10^4	1.7×10^4	1.2×10^4	1.2×10^4
	n_0 [b] ($\rm cm^{-3}$)	16×10^6	1.2×10^6	1.6×10^6	5.2×10^5	3.3×10^5
	r_0 [c] (AU)	10^3	5.4×10^3	3.4×10^3	4×10^3	7×10^3
	$A_V^{\rm cloud}$ [d]	0.19	0.35	2.8	0.45	0.17
	$d_\star$ [e] (pc)	1.1	1.4	1.3	1.8	1.6
	M [f] ($\rm M_\odot$)	24	61	18	47	14
	$A_V^{\rm clump}$ [g]	1090	400	560	120	130
(II)	$T_{\rm centre}$ [h] (K)	6	7	7	7	8
	$T_{\rm edge}^{\rm min}$ [i] (K)	14	13	12	14	14
	$T_{\rm edge}^{\rm max}$ [j] (K)	27	22	14	20	24
	$\lambda_{\rm peak}$ [k] (μm)	125	200	270	200	160

[a] Clump extent.
[b] Clump central number density.
[c] Flattening radius of each clump.
[d] Visual extinction through the ambient cloud.
[e] Distance of each clump from HD147889
[f] Clump mass (calculated from the density profile assumed and the extent of the clump).
[g] Visual extinction to the centre of each clump (calculated from the density profile assumed and the extent of the clump).
[h] Temperature at the centre of the clump.
[i] Temperature at the edge of the clump facing away from the H147989 direction.
[j] Temperature at the edge of the clump facing towards H147989.
[k] Wavelength of the peak of the computed SED

For the stellar radiation we adopt the parameters computed by Liseau et al. (1999) ($T_\star^{\rm eff}=22,000$ K, $R_\star=5$ $\rm R_\odot$, $L_\star=5,300$ $\rm L_\odot$). We shall assume that this star emits as a blackbody having temperature 22,000 K. Due to the presence of this star in the vicinity of ρ Oph, the external heating of the clumps is highly anisotropic.

For the external interstellar radiation field we adopt a revised version of the Black (1994) interstellar radiation field (BISRF). The BISRF consists of radiation from giant stars and dwarfs, thermal emission from dust grains, cosmic background radiation, and mid-infrared emission from transiently heated small PAH grains (André et al. 2002). This radiation field is modulated by the ambient cloud around each clump, hence the incident radiation field on each of the clumps is enhanced at FIR and longer wavelengths, and attenuated a shorter wavelengths.

The geometry of the ρ Oph region is taken from the 3D model constructed by Liseau et al. (1999) based on far infrared spectrophotometric observations with the ISO-LWS. Using this model and the 1.3mm mosaic image of Motte et al. (1998), we estimate the distance of HD147889 from each of the ρ Oph clumps (see Table 1). These are rough estimates but they do not greatly affect the results of the model.

3.4 Monte Carlo radiative transfer

The radiative transfer calculations are performed using PHAETHON, a 3D Monte Carlo radiative transfer code developed by Stamatellos & Whitworth (2003). The code uses a large number of monochromatic luminosity packets to represent the radiation sources in the system. The luminosity packets are injected into the cloud and interact (are absorbed, reemitted, scattered) stochastically with it. If an L-packet is absorbed its energy is added to the local region and raises the local temperature. To ensure radiative equilibrium the L-packet is re-emitted immediately with a new frequency chosen from the difference between the local cell emissivity before and after the absorption of the packet (Bjorkman & Wood 2001; Baes et al. 2005).

The model for each ρ Oph clump is essentially 2-dimensional, hence the code used here is adapted and optimised for the study of systems with azimuthal symmetry. Each clump is divided into a number of cells by spherical and conical surfaces. The spherical surfaces are evenly spaced in radius, and there are typically 100 of them. The conical surfaces are evenly spaced in polar angle, and there are typically 40 of them. Hence, each clump is divided into ~ 4000 cells. The number of cells used is chosen so that the density and temperature differences between adjacent cells are small.

The L-packets representing the ambient radiation field (typically a few 10^{10} packets) are injected from the outside of the clump with injection points and injection directions chosen to mimic an isotropic radiation field incident on the ambient cloud around each clump (Stamatellos et al. 2004).

The L-packets representing the stellar radiation from HD147889 (typically a few 10^{10} packets are used) are emitted from the star with random direction and only a fraction of them ($\sim 1\%$) heats the clumps. However, due to the large luminosity of HD147889, this small percentage of stellar photons dominates over the background radiation field.

4 DUST TEMPERATURES AND SEDS OF THE CLUMPS IN THE ρ OPH MAIN CLOUD

The optical depth of the virtual ambient cloud around each clump is varied so that to produce an SED for each clump that peaks at a wavelength corresponding to a dust temperature that matches the dust temperature assumed by previous authors. In the next subsections we present the dust temperature profiles and the SEDs of each clump as calculated by this model (see Figs. 3-7).

4.1 ρ Oph A

Oph A is, according to the Liseau et al. (1999) 3D model, the closest clump to HD147889. The radiation from the star dominates over the interstellar radiation field and heats the clump to temperatures that range from $6-7$ K in the centre of the clump, to $13-27$ K at the clump edge (Fig. 3). The clump hemisphere closer to the star has higher temperatures (up to 27 K) than the other hemisphere, which has temperature not higher than 15 K. In total, 80% of the clump volume is colder than 15 K. The ambient cloud has dust temperatures 30-40 K on the side closer to the star, which are consistent with previous temperature estimates based on the PDR model of Liseau et al. (1999).

The SED of the model of ρ Oph A (Fig. 3b) peaks at around 125 μm, which is suggestive of a temperature[2] around $\sim$ 20 K. This value is consistent with what other studies have indicated (e.g. André et al. 1993) about the temperature derived from the SED. However, the peak of the SED peaks at this wavelength due to the contribution from the outer hotter parts of the clump, whilst most of the clump is colder. The region of the clump where prestellar cores are observed, i.e. at visual extinctions $A_{\rm V} > 7$ mag (according to Johnstone et al. 2004), is colder than 11 K.

4.2 ρ Oph B-2

The temperature profile of the ρ Oph B-2 clump (Fig. 4) is similar to that of Oph A. This clump is colder than Oph A, and its temperature drops from $13-23$ K at the edge of the cloud to $\sim$ 7 K at its centre. The SED distribution of the clump peaks at around 195 μm indicating a temperature of 13 K, which is consistent with previous observations. As in Oph A, the SED peak is characteristic of the outer warmer layers, whereas most of the clump is colder than 13 K. Again assuming that cores are observed at visual extinctions $A_{\rm V} > 7$ mag, we find that their temperatures should be below 10 K.

4.3 ρ Oph C

The estimated temperature of this clump from previous observations is around 10 K (e.g. Motte et al. 1998; André et al. 1993). This clump is colder than the previous two, suggesting that it is shielded from HD147879, possibly by parts of the other ρ Oph clumps. The temperature of this clump drops from 11-13 K at its edge of to 6-7 K at its centre (Fig. 5a). The SED of the system peaks at around 270 μm (Fig. 5b), which corresponds to a temperature of 9 K. Assuming that cores exist at visual extinctions $A_{\rm V} > 7$ mag we find that their temperatures should be below 10 K.

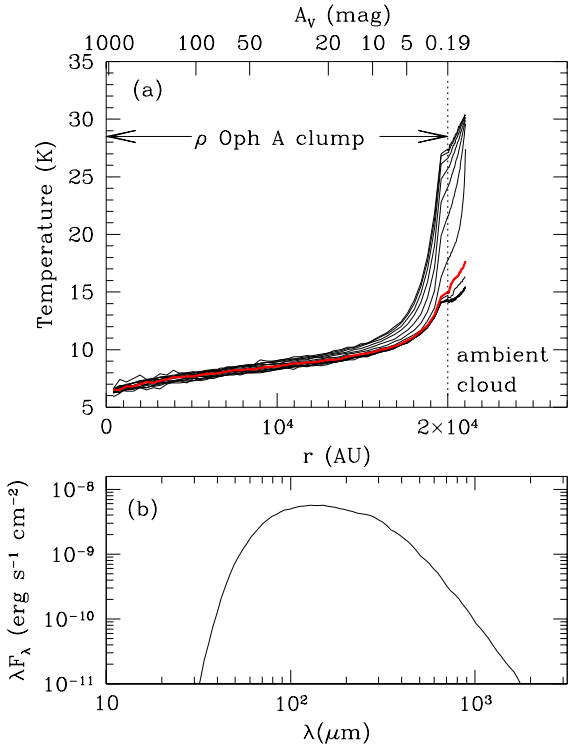

Figure 3. (a) Dust temperature profile of the Oph-A clump versus the distance from its centre, and versus visual extinction from the surface of the clump. We plot the radial temperature profile from $\theta = 0°$ to 180° to every 9°, where $\theta = 0°$ corresponds to the direction towards the B2V star. The red thick line corresponds to the direction perpendicular to the clump-star direction (red thick strip in Fig. 1). **(b)** Simulated SED of the clump.

4.4 ρ Oph D

The temperature profile and the SED of ρ Oph D are presented in Fig. 6. The SED peaks at around 205 μm, corresponding to a temperature of 12 K, as assumed by Motte et al. (1998). However, most of the clump is colder than 12 K. Assuming that cores exist at visual extinctions$A_{\rm V} > 7$ mag we find that their temperature should be below 10 K.

4.5 ρ Oph F

The temperature profile and the SED of ρ Oph F are presented in Fig. 7. The SED peaks at around 160μm, corresponding to a temperature of 16 K. However, most of the clump is colder than 16 K, with the region at visual extinctions $A_{\rm V} > 7$ mag having temperature below 10 K.

4.6 Dust heating by young protostars

We have so far ignored heating from nearby young protostars. Motte et al. (1998) identify a number of Class 0, Class

[2] We note that the peak of SED corresponds to the peak of $\lambda\, k_\lambda B_\lambda$, which for $k_\lambda \propto \lambda^{-1.78}$, i.e. the Ossenkopf & Henning (1994) opacity, translates to $\lambda_{\rm peak}T \approx 2,500$ K μm.

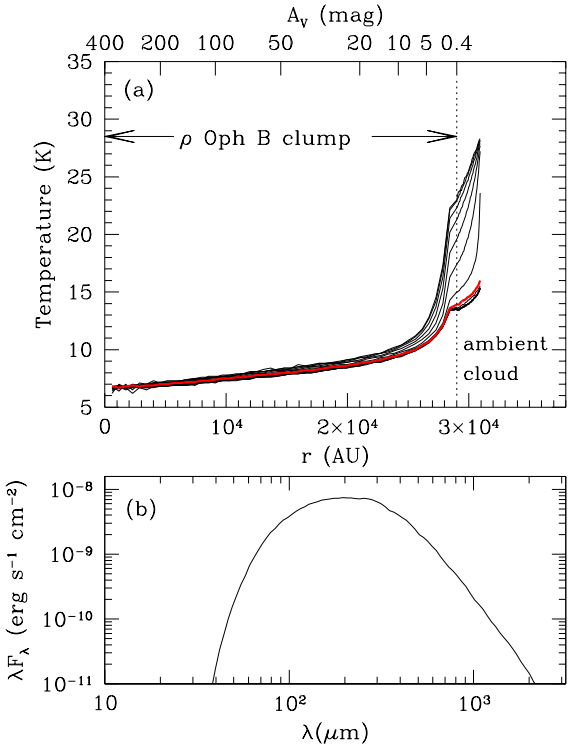

Figure 4. Same as in Fig. 3 but for the Oph-B2 clump.

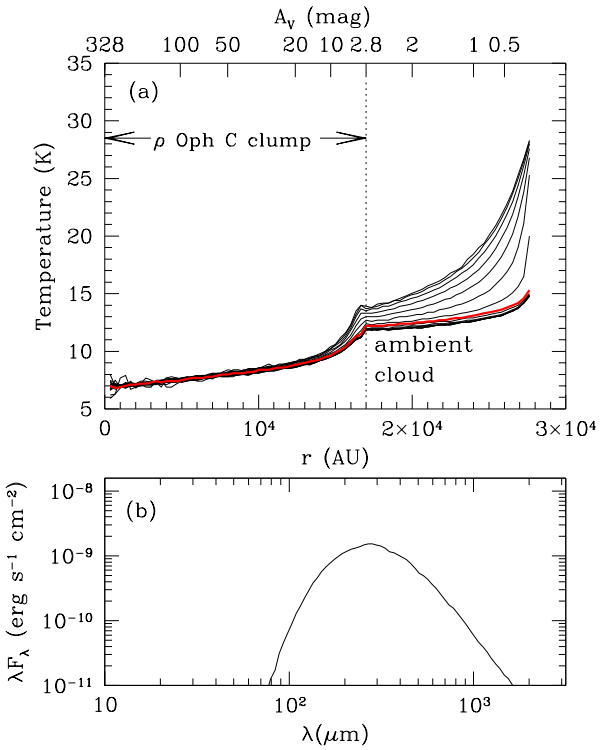

Figure 5. Same as in Fig. 3 but for the Oph-C clump

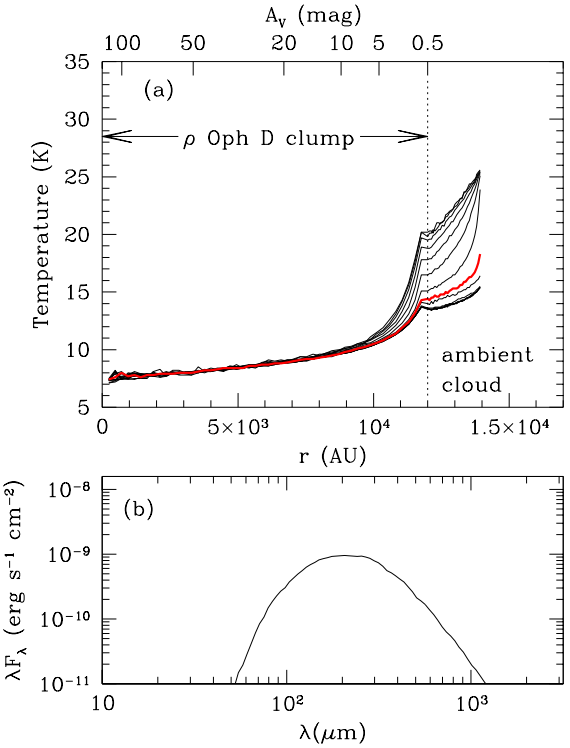

Figure 6. Same as in Fig. 3 but for the Oph-D clump.

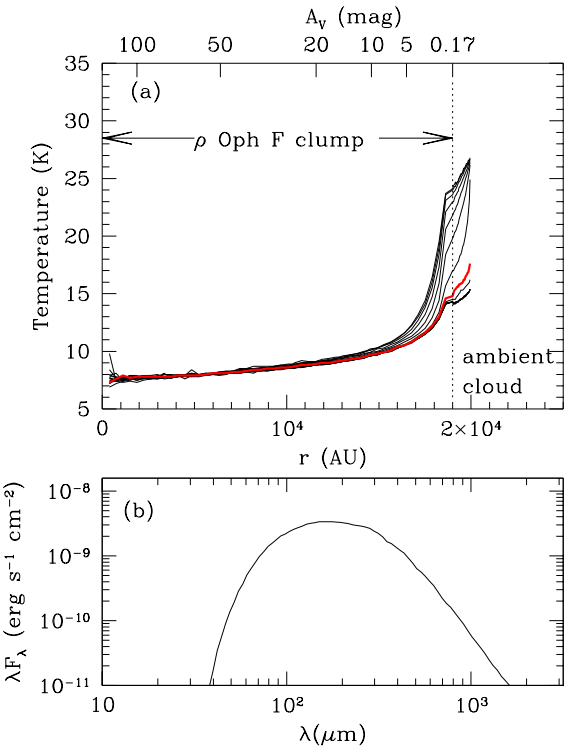

Figure 7. Same as in Fig. 3 but for the Oph-F clump.

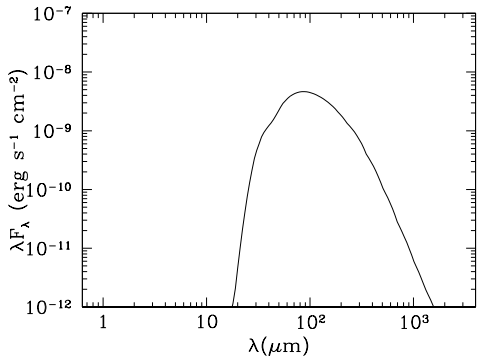

Figure 8. SED of a young Class 0 object as calculated by Stamatellos et al. (2005), assuming a distance of 160 pc. The bolometric luminosity of this source is 5 $L_{\odot}$.

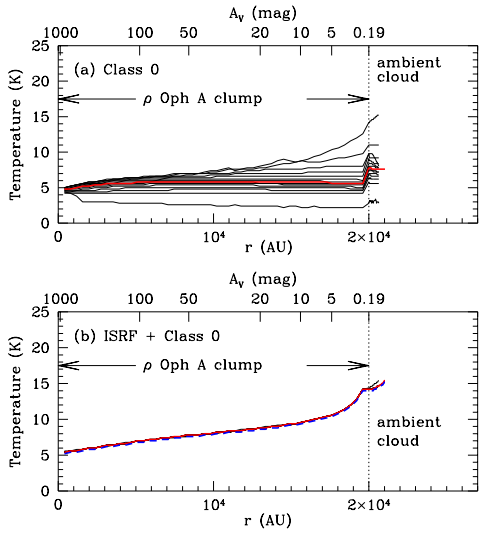

Figure 9. (a) Dust temperature profile of the clump, in different directions, due to heating from a Class 0 object at the edge of the clump (b) Dust temperature profile, in different directions, due to heating from a Class 0 object and the interstellar radiation field. The thick (red) line corresponds to the direction perpendicular to the clump-protostar direction. The dashed (blue) line corresponds to the temperature when only heating from the ISRF is considered. The role ISRF is dominant.

I and Class II objects either near the clumps or embedded in the clumps. The presence of these luminosity sources is expected to increase the clump temperature. In order to quantify this increase we use the ρ Oph A clump as a study case, and consider heating (i) from a Class 0 object located at the edge of the clump, (ii) from a Class I object also located at the edge of the clump, and (iii) from a Class I object embedded in the clump, 0.05 pc from its centre. The SEDs of the Class 0 and the Class I objects are taken from the simulations of Stamatellos et al. (2005) (Figs. 8, 10). The bolometric luminosity (i.e. the integrated luminosity over the entire spectrum) of the Class 0 source is 5 $L_{\odot}$, and that of the Class I source is 10 $L_{\odot}$. These are typical luminosities of such objects in the region (e.g. Wilking et al. 1989).

The results of the radiative transfer simulations are presented in Figs. 9, 11, and 12. On the top graph of each figure we present the dust temperature taking into account only the heating from the nearby or the embedded source. The

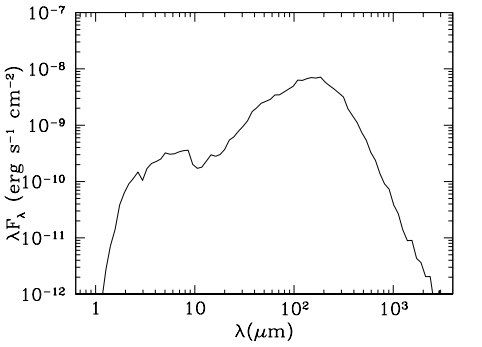

Figure 10. SED of a young Class I object as calculated by Stamatellos et al. (2005), assuming a distance of 160 pc. The bolometric luminosity of this source is 9.3 $L_{\odot}$.

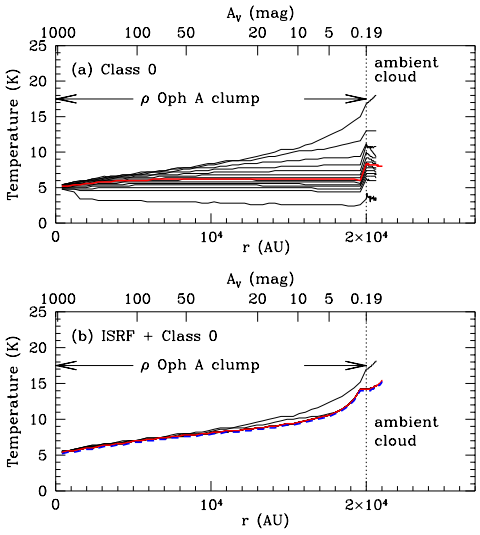

Figure 11. Same as in Fig. 9, but for heating from a Class I object at the edge of the clump. The ISRF is again dominant.

clump is hotter closer to the assumed source, as expected, with the temperature ranging from 4 to 15 K in different directions inside the clump. On the bottom graphs of each figure we present the dust temperature also taking into account the heating of the ISRF, which has a bolometric luminosity of 5 $L_{\odot}$, i.e. comparable with the luminosities of the nearby or embedded sources. As seen in the figures the role of the ISRF is dominant; the presence of the nearby Class 0 object does not affect the dust temperature at all, and the presence of a nearby Class I object just heats the outer layers of the clump that are closer to it by only ~ 2 K. The presence of an embedded Class I object is more noticeable. It increases the dust temperature in the clump by $\sim 1-2$ K, and very close to it by ~ 5 K. However, we note that (i) the temperature of most of the clump is still below 10 K, and (ii) the increase of temperature is not greater than the increase of temperature when the radiation from HD147889 is considered (cf. Fig. 3b). This is because (i) the luminosity of the protostar is comparable to the luminosity of the ISRF, hence smaller than the luminosity of HD147889 reaching the clump, and (ii) most of the protostar's radiation is emitted at long wavelengths, where the clump is optically thin.

We conclude that the effect of heating due to the presence of nearby or embedded young protostars is not greater

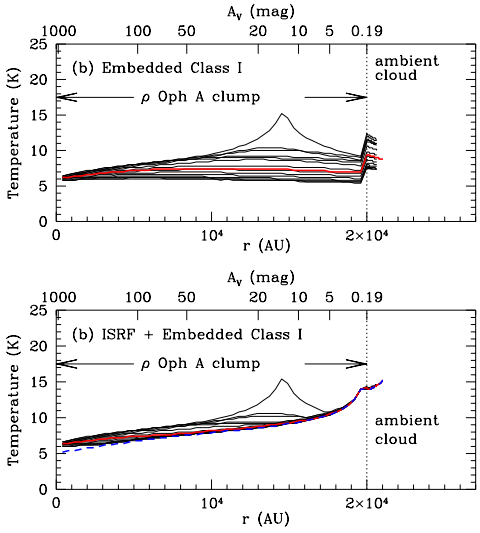

Figure 12. Same as in Fig. 9, but for heating from a Class I object located inside the clump (0.05 pc away from the centre of the clump). The heating provided by the ISRF is still dominant apart from the region close to the embedded protostar.

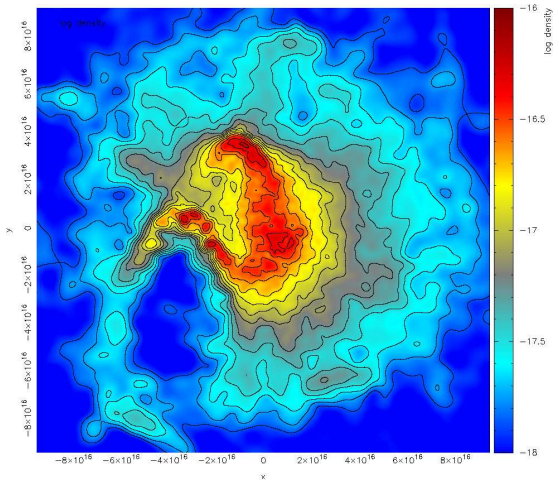

Figure 13. Logarithmic density (in g cm^{-3}) on the $x-y$ plane of a simulated Oph A-like clump. The density ranges from 10^{-18} to 10^{-16} g cm^{-3}. x and y are given in cm.

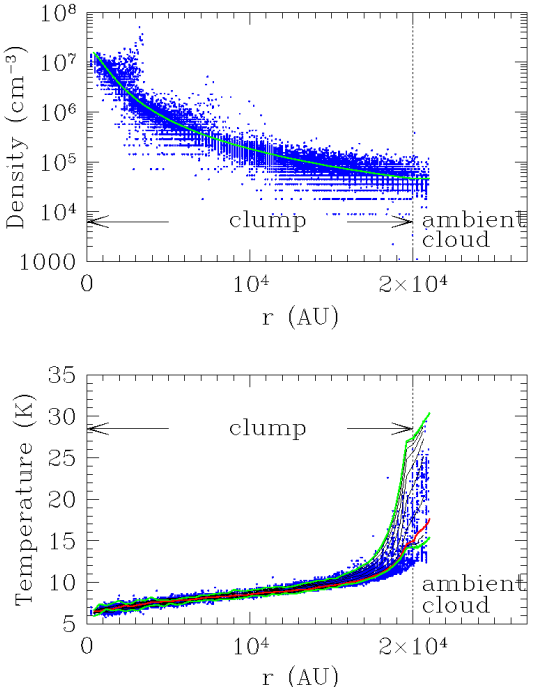

Figure 14. Density and temperature profiles (dots) of the simulated clump of Fig. 13. Each dot corresponds to the temperature of each radiative transfer cell constructed from the output of the SPH simulation. The density and temperature profiles of the spherically symmetric model are also plotted (lines). The upper green line corresponds to the direction towards HD147889 and the lower green line to the opposite direction. The dust temperature in the case of a 3D clumpy structure is similar to the temperature calculated using the spherical symmetric model.

than the effect of the ISRF, and hence secondary to the effect of HD147889. Thus, nearby or embedded young protostars do not greatly affect the dust temperatures in the regions deep inside the clumps where prestellar cores are observed, unless there is a large number of young protostars within each clump, which is not the case for the ρ Oph main cloud.

4.7 The effect of a 3D clumpy structure

In the radiative transfer simulations presented so far we use spherically symmetric models to describe the big clumps in the ρ Oph main cloud. In reality these clumps are more structured, as they contain regions where the density is either higher or lower than the assumed spherically symmetric model. Indebetouw et al. (2006) examined the effect the cloud clumpiness in the case of clouds that contain high-mass stars and they found that the dust temperature is affected significantly due to the clumpiness of the medium.

To examine the effect of the 3D clumpy structure of the regions of the ρ Oph main cloud, we generate a 3D ρ Oph-A-like clump as follows. We start off with a spherically symmetric clump with the parameters adopted for ρ Oph-A (see Table 1). We then impose a turbulent velocity field (e.g. Goodwin et al. 2004), and use DRAGON, an SPH code, to follow the evolution of the cloud. Due to the effect of turbulence the cloud acquires a clumpy structure. The cloud is evolved until cores are formed (Figs. 13, 14). We then perform a radiative transfer simulation on the clumpy structure using the method of Stamatellos & Whitworth (2005a). As in the previous sections we consider heating both by the ISRF and HD147889. The calculated temperature profile is presented in Fig. 14. The dust temperature is similar to the temperature calculated in the spherically symmetric case, despite the fact that the density in some regions of the cloud is up to an order of magnitude different. This is because the heating of the dense parts of the cloud is mainly due to long wavelength radiation that propagates into the cloud without "seeing" the clumpy structure; short wavelength radiation is absorbed in the outer layers of the cloud and re-emitted at longer wavelengths.

We conclude that the clumpiness of the cloud does not significantly affect the dust temperature at the inner, dense regions of the cloud.

4.8 The dust temperature of the cores in the ρ Oph main cloud

According to the model presented here, the dust temperatures of the cores in ρ Oph main cloud are lower than previously thought. Since cores are observed at visual extinctions > 7 mag, the temperatures of the cores in Oph-A are most probably below 11 K, and in Oph-B2, Oph-C, Oph-D and Oph-F below 10 K. These temperatures correspond to the temperature of the clumps where the cores are embedded, at visual extinctions $A_{\rm V} = 7$ mag.

Considering the fact that most of the cores are observed at visual extinctions $12 - 20$ mag (Johnstone et al. 2004), their actual temperatures may be even lower by $\sim$ 2 K. Hence, the presence of the luminous HD147889 in the vicinity of the clumps, affects only the outer regions of the clumps, where prestellar cores have not been observed.

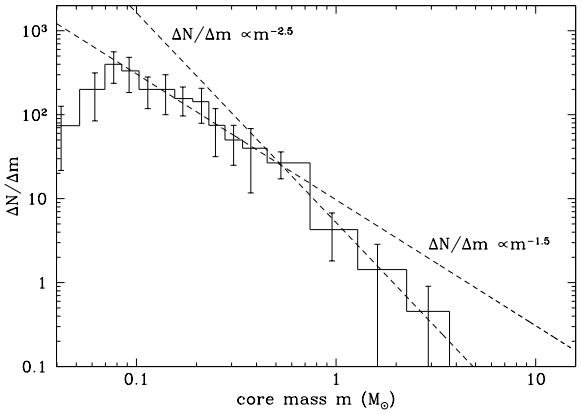

Figure 15. The core mass function of the ρ Oph main cloud based on the core masses calculated by Motte et al. (1998). The error bars correspond to $\sqrt{N}$ counting statistics

5 THE CORE MASS FUNCTION OF ρ OPH

Motte et al. (1998) calculated the core mass function of the ρ Oph main cloud by assuming a temperature of 20 K for Oph-A, 12 K for Oph-B, Oph-C, and Oph-D, and 15 K for Oph-E and Oph-F. Johnstone et al. (2000) have assumed similar temperatures to Motte et al. (1993) or even higher temperatures. These temperatures are higher than the ones predicted by our model, by $2 - 9$ K. Hence, considering the fact that core masses are calculated using Eq. 1, we suggest that both these authors have underestimated the masses of the prestellar cores in this region. At these temperatures the Rayleigh-Jeans relation is not a good approximation and the Planck function must be used; hence even overestimating temperatures by a few K leads to underestimating masses by a factor of $2 - 3$.

We revise the core mass function of Motte et al. (1998) assuming core temperatures derived from our model (Section 4.8). We shall assume the same dust opacity at 1.3 mm, i.e. $\kappa = 0.005$ cm^2 g^{-1} (Preibisch et al. 1993; André et al. 1996). We then calculate the core the core masses from the observed fluxes using Eq 1. We note again that temperatures we assume correspond to cores at visual extinctions of ~ 7 mag. Johnstone et al. (2004) suggest that most of the cores in this region are embedded at $12 - 21$ mag or at even higher extinctions. Hence the temperatures of many of the cores are expected to be even lower (by ~ 2 K). This means that the temperatures used are upper limits to the actual temperatures, and consequently that the computed masses are lower limits to the actual core masses.

In Fig. 15 we present the Motte et al. (1993) CMF, and in Fig. 16 the revised CMF derived using core temperatures from the model presented in this paper. The CMF has moved to higher masses but its overall shape has not changed significantly. The mass at which the core mass spectrum steepens from a slope $\alpha \sim 1.5$ to a slope $\alpha \sim 2.5$ is less clear in this case but it seems that it has moved from ~ 0.5 M$_\odot$ to ~ 1 M$_\odot$. Contrary to the CMF in other star forming regions (e.g. in Orion; Nutter et al. 2007) the CMF does not show a turnover down to the completeness limit (which is ~ 0.2 M$_\odot$, using the new temperatures). However, the CMF may flatten at around ~ 0.4 M$_\odot$.

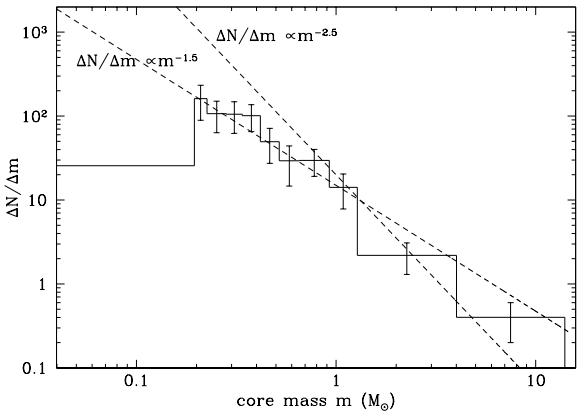

Figure 16. The CMF of the ρ Oph main cloud based on the core masses calculated using temperatures from our model. The CMF is constructed so that there is approximately equal number of cores per bin. The CMF has moved to larger masses but its overall shape has not changed significantly.

6 DUST TEMPERATURES OF CORES IN OTHER STAR FORMING REGIONS

The dust temperatures of prestellar cores are determined by the ambient radiation field heating the core (since by definition there are no radiation sources inside the core). This radiation field is determined by environmental factors. It depends (i) on how deeply the core is embedded in its ambient cloud, and (ii) on the possible presence of nearby radiation sources, and their relative position/distance with respect to the core. Hence, the external radiation field that heats each core is different.

Previous studies of prestellar cores and young protostars (e.g. Evans et al. 2001; Young et al. 2003; Jorgensen et al. 2006) have acknowledged this fact and have used a scaled version of the standard ISRF that is either enhanced at all wavelengths or selectively at UV and FIR. This simple approach has a free parameter, the ISRF scaling factor, which is varied arbitrarily to fit the observations but it is not connected directly to the molecular cloud in which the core is embedded or the transport of radiation inside the cloud.

It also does not account for the fact that the radiation field incident on an embedded core is not isotropic.

Here, we follow the approach of Stamatellos et al. (2004) where the radiation field incident on the core is a direct result of the presence (i) of the ambient cloud that surrounds the core, (ii) of nearby embedded young protostars, (iii) of nearby luminous stars. The ambient cloud of each core/clump attenuates the ISRF, as it acts like a shield to UV, visual and NIR interstellar radiation, absorbing and re-emitting it in the FIR. The nearby young protostars and stars also enhance the radiation field incident on core, mainly at long wavelengths (> 50 μm) due to the thermal emission from the outer regions of the heated ambient cloud (Mathis et al. 1983), as short wavelength radiation cannot penetrate deep into the cloud.

6.1 Dust temperatures of the prestellar cores in the ρ Oph molecular cloud

In the previous sections we discussed in detail the region of the ρ Oph main cloud, where the external heating is dominated by a nearby B2V star. Due to the presence of this star and embedded protostars in the ρ Oph main cloud the external radiation field is stronger than the standard ISRF by a factor of ~ 10 (the bolometric luminosity of the ISRF heating the core is ~ 5 $L_{\odot}$ whereas the bolometric luminosity of the star's radiation reaching and heating each clump is ~ 50 $L_{\odot}$). This is consistent with the observations of Liseau et al. (1999) which suggest that the external radiation field incident on ρ Oph $\sim 10-100$ times stronger than the standard ISRF.

Using a detailed model presented in the previous sections, we estimate that the temperatures of the cores in the ρ Oph main cloud are probably below 10-11 K, i.e. lower than previous estimates. The dust temperatures of the cores in L1689, another region of the Ophiuchus molecular cloud which is totally starless (e.g. Nutter et al. 2006), are also probably below 10-11 K.

6.2 Dust temperatures of the prestellar cores in the Taurus molecular cloud

In Taurus there are no nearby luminous stars, hence the radiation field heating the cores in this region is enhanced only due to the presence of young protostars and stars in its vicinity. This radiation field is not expected to be stronger than that in ρ Oph. Thus, the dust temperatures estimated by our model for the ρ Oph main cloud are upper limits to the temperatures of the cores in Taurus. Indeed, observations of TMC-1C, a prestellar core in in Taurus (Schnee & Goodman 2005; Schnee et al. 2006), suggest dust temperatures that drop from 11 K at the edge of the core ($A_{\rm V} \approx 10$) to 5 K at its centre ($A_{\rm V} \approx 80$), which are consistent with heating from an ISRF that is weaker than the standard ISRF.

In Fig. 17 we present a model for TMC-1C. Based on the estimates from Schnee et al. (2006) we assume the density profile defined in Eq. 2, with $r_0 = 0.02$ pc, $n_0 = 5.5 \times 10^5$ cm^{-3} and $R_{\rm core} = 15000$ AU. We further assume a virtual ambient cloud around the core of visual extinction $A_{\rm V} = 3.5$. This virtual cloud modifies the radiation field incident on the core. The calculated temperature

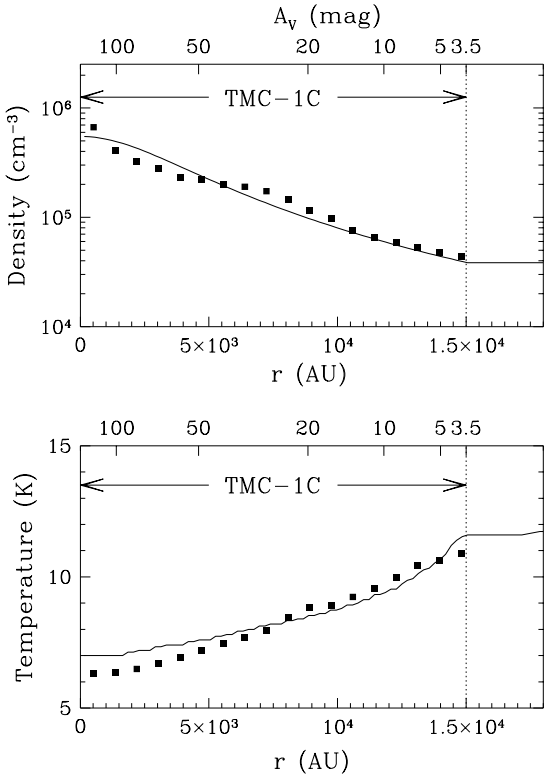

Figure 17. Assumed density profile and calculated temperature profile of TMC-1C (solid lines) in Taurus. The squares correspond to estimates based on observations at 450 μm, 850 μm, and 1200 μm (Schnee et al. 2007).

(Fig. 17, bottom) is very similar to the temperature estimated by Schnee et al. (2006). The calculated temperature at the centre of the core is higher by ~ 1 K than the Schnee et al. (2006) estimate, indicating that the radiation field heating the core is weaker than the standard ISRF at long wavelengths (or alternatively that the core centre is denser).

We conclude that the dust temperatures of the prestellar cores in Taurus are probably below 10 K.

6.3 Dust temperatures of the prestellar cores in the Orion molecular cloud

In Orion there are many radiation sources that contribute to the heating of the prestellar cores in region. Jorgensen et al. (2006) estimates that the external radiation field in the Orion region is up to $\sim 10^3$ stronger than the standard interstellar radiation field.

In order to investigate the effect of such an enhanced radiation field on the dust temperatures in prestellar cores in Orion, we use ρ Oph A as a representative clump, and consider heating from a B2V star (similar to HD147889) with different temperatures and at different distances from the centre of the clump. Hence, we examine the effect of heating from an incident radiation field having bolometric luminosity $L_{\rm H}$ 10, 20, 50, 120, 500 and 10^3 times the bolometric luminosity of the standard interstellar radiation field (Black 1994; André et al. 2002).

In Fig. 18 we present the dust temperature versus visual extinction calculated using incident radiation fields of

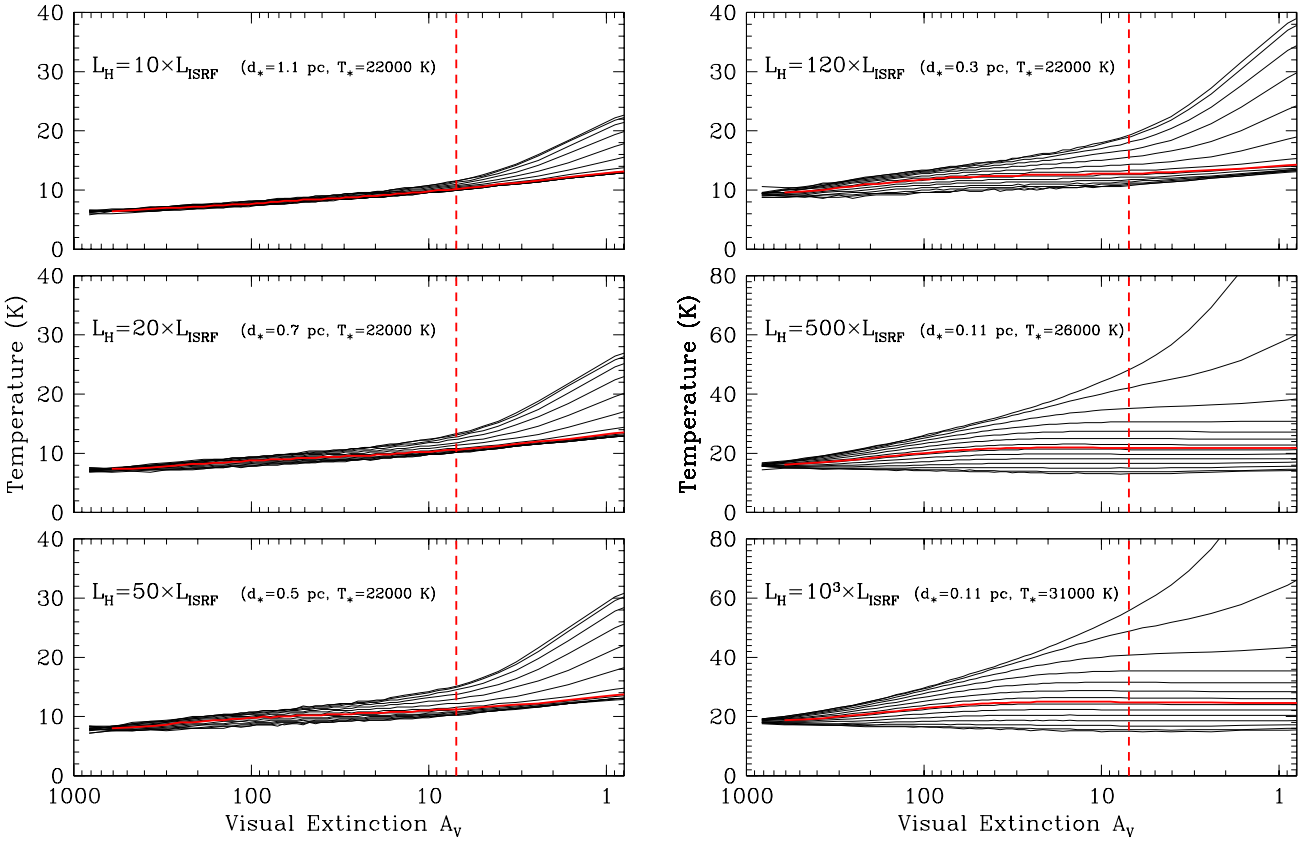

Figure 18. Dust temperature of a ρ Oph A-like clump against the visual extinction from the edge of the clump. The clump heating is due to the ISRF and a B2V star having different distances from the centre for the clump and different temperatures, so as to change the bolometric luminosity incident on the clump (as marked on each graph). The temperature of most of the clump is below 10 K unless the heating from the star is very strong ($\gtrsim 120 \times L_{\rm ISRF}$).

different strengths. For radiation fields with bolometric luminosities up $50 \times L_{\rm ISRF}$ the dust temperature profile is similar to the ones calculated for ρ Oph; most of the dust at optical visual extinctions > 7 mag is colder than 10 K. For a radiation field $120 \times L_{\rm ISRF}$, half of the clump (i.e. the hemisphere away from the luminosity source) is colder than 12 K. For a higher external radiation, $(500 - 10^3) \times L_{\rm ISRF}$, the dust temperature in the clump varies considerably with the position in the clump; from 14 to 45 K in the case of $500 \times L_{\rm ISRF}$, and from 15 to 53 K for the case of $10^3 \times L_{\rm ISRF}$. Hence, the dust temperature of a core depends on the core position in the clump, i.e. its relative position with respect to the external radiation source and on how deeply embedded the source is in its parent cloud.

We conclude that assuming that (i) the incident radiation field on the clumps of Orion is $(500 - 10^3) \times L_{\rm ISRF}$, and (ii) that cores exist at visual extinctions > 7 mag, then typical dust temperatures of the prestellar cores in Orion are from 20 to 30 K, which is consistent with previous assumptions/estimates (Launhardt et al. 1996; Mitchell et al. 2001; Motte et al. 2001; Johnstone et al. 2006; Nutter et al. 2007).

7 CONCLUSIONS

We have used a 3D geometry for the ρ Oph main cloud region to construct a radiative transfer model for this region, taking into account external heating by (i) the interstellar radiation field, and (ii) HD147889, a nearby B2V star. HD147889 dominates the heating of the ρ Oph main cloud clumps. We estimate that the dust temperatures at visual extinctions > 7 mag are below ∼10-11 K. These are smaller than was previously assumed. As a result we find that the core masses calculated from mm observations are underestimated by a factor of 2-3. This affects the core mass function of the ρ Oph main cloud. We computed a revised CMF for this region using the dust temperatures calculated in this paper. The CMF has moved to higher masses but its shape has not changed significantly. The mass at which the core mass spectrum steepens from a slope $\alpha \sim 1.5$ to a slope $\alpha \sim 2.5$ is less clear but it appears that it has moved from ~ 0.5 M$_\odot$ to ~ 1 M$_\odot$. This is still below the mass where this steepening occurs in Orion. Contrary to the CMF in Orion the CMF of the ρ Oph main cloud does not show a turnover at low masses. However, it may flatten at around ~ 0.4 M$_\odot$.

We have generalized our study to estimate the dust temperatures in prestellar cores in other star forming regions. In the Taurus molecular cloud the ambient radiation field is weaker than that in Ophiuchus, hence the dust temperatures

of the cores in this region are similar or smaller than the ones calculated for ρ Oph. We estimate that the dust temperatures at visual extinctions > 7 mag are below $\sim$10 K. In Orion the ambient radiation field is estimated to be up to 10^3 times stronger than the standard interstellar radiation field. Using a simple model to account for this enhanced radiation field, we find that the typical dust temperatures of the prestellar cores in this region are from 20 to 30 K.

ACKNOWLEDGEMENTS

We would like to thank S. Schnee for providing the data for TMC-1C, and P. Andrè for providing an improved version of the BISRF. We also thank J. Kirk and D. Nutter for useful discussions on prestellar cores in Taurus and Orion, and R. Simpson for Fig. 15. We acknowledge support by PPARC grant PPA/G/O/2002/00497.

REFERENCES

Alves, J., Lada, C. J., & Lada, E. A. 2001, Nature, 409, 159
André, P., & Montmerle, T. 1994, ApJ, 420, 837
André, P., Ward-Thompson, D., & Barsony, M. 1993, ApJ, 406, 122
André, P., Ward-Thompson, D., & Motte, F. 1996, A&A, 314, 625
André, P., Bouwman, J., Belloche, A., & Hennebelle, P. 2003, SFChem 2002: Chemistry as a Diagnostic of Star Formation, proceedings of a conference held August 21-23, 2002 at University of Waterloo, Waterloo, Ontario, Canada N2L 3G1. Edited by Charles L. Curry and Michel Fich. NRC Press, Ottawa, Canada, 2003, p. 127., 127
André, P., Ward-Thompson, D., & Barsony, M. 2000, Protostars and Planets IV, 59
Bacmann, A., André, P., Puget, J.-L., Abergel, A., Bontemps, S., & Ward-Thompson, D. 2000, A&A, 361, 555
Baes, M., Stamatellos, D., Davies, J. I., Whitworth, A. P., Sabatini, S., Roberts, S., Linder, S. M., & Evans, R. 2005, New Astronomy, 10, 523
Bjorkman, J. E. & Wood, K. 2001, ApJ, 554, 615
Black, J. H. 1994, ASP Conf. Ser. 58: The First Symposium on the Infrared Cirrus and Diffuse Interstellar Clouds, 355
Bonnor, W. B. 1956, MNRAS, 116, 351
Bontemps, S., et al. 2001, A&A, 372, 173
di Francesco, J., Evans, N. J., II, Caselli, P., Myers, P. C., Shirley, Y., Aikawa, Y., & Tafalla, M. 2007, Protostars and Planets V, 17
Draine, B. T. 2003, ARA&A, 41, 241
Ebert, R. 1955, Zeitschrift für Astrophysics, 37, 217
Evans, N. J., II, Rawlings, J. M. C., Shirley, Y. L., & Mundy, L. G. 2001, ApJ, 557, 193
Goodwin, S. P., Whitworth, A. P., & Ward-Thompson, D. 2004, A&A, 414, 633
Hildebrand, R. H. 1983, QJRAS, 24, 267
Indebetouw, R., Whitney, B. A., Johnson, K. E., & Wood, K. 2006, ApJ, 636, 362
Johnstone, D., Wilson, C. D., Moriarty-Schieven, G., Joncas, G., Smith, G., Gregersen, E., & Fich, M. 2000, ApJ, 545, 327
Johnstone, D., Di Francesco, J., & Kirk, H. 2004, ApJ, 611, L45
Johnstone, D., Matthews, H., & Mitchell, G. F. 2006, ApJ, 639, 259
Jørgensen, J. K., Johnstone, D., van Dishoeck, E. F., & Doty, S. D. 2006, A&A, 449, 609
Kirk, J. M., Ward-Thompson, D., & André, P. 2005, MNRAS, 360, 1506
Kirk, H., Johnstone, D., & Di Francesco, J. 2006, ApJ, 646, 1009
Lada, C. J. 1987, IAU Symp. 115: Star Forming Regions, 115, 1
Launhardt, R., Mezger, P. G., Haslam, C. G. T., Kreysa, E., Lemke, R., Sievers, A., & Zylka, R. 1996, A&A, 312, 569
Liseau, R. et al. 1999, A&A, 344, 342
Mathis, J. S., Mezger, P. G., & Panagia, N. 1983, A&A, 128, 212
McKee, C. F. 1989, ApJ, 345, 782
Mitchell, G. F., Johnstone, D., Moriarty-Schieven, G., Fich, M., & Tothill, N. F. H. 2001, ApJ, 556, 215
Motte, F., André, P., & Neri, R. 1998, A&A, 336, 150
Motte, F., André, P., Ward-Thompson, D., & Bontemps, S. 2001, A&A, 372, L41
Myers, P. C. & Benson, P. J. 1983, ApJ, 266, 309
Nutter, D., Ward-Thompson, D., & André, P. 2006, MNRAS, 368, 1833
Nutter, D., & Ward-Thompson, D. 2007, MNRAS, 374, 1413
Ossenkopf, V. & Henning, T. 1994, A&A, 291, 943
Preibisch, T., Ossenkopf, V., Yorke, H. W., & Henning, T. 1993, A&A, 279, 577
Ridge, N. A., et al. 2006, AJ, 131, 2921
Schnee, S., & Goodman, A. 2005, ApJ, 624, 254
Schnee, S., Kauffmann, J., Goodman, A., & Bertoldi, F. 2006, ArXiv Astrophysics e-prints, arXiv:astro-ph/0611535
Stamatellos, D. & Whitworth, A. P. 2003a, A&A, 407, 941
Stamatellos, D., & Whitworth, A. P. 2003b, ASSL Vol. 299: Open Issues in Local Star Formation, 347
Stamatellos, D., Whitworth, A. P., André, P., & Ward-Thompson, D. 2004, A&A, 420, 1009
Stamatellos, D., & Whitworth, A. P. 2005a, A&A, 439, 153
Stamatellos, D., & Whitworth, A. 2005b, ASSL Vol. 327: The Initial Mass Function 50 Years Later, 319
Stamatellos, D., Whitworth, A. P., Boyd, D. F. A., & Goodwin, S. P. 2005, A&A, 439, 159
Ward-Thompson, D., Scott, P. F., Hills, R. E., & Andre, P. 1994, MNRAS, 268, 276
Ward-Thompson, D., Motte, F., & André, P. 1999, MNRAS, 305, 143
Ward-Thompson, D., André, P., & Kirk, J. M. 2002, MNRAS, 329, 257
Ward-Thompson, D., André, P., Crutcher, R., Johnstone, D., Onishi, T., & Wilson, C. 2007, Protostars and Planets V, 33
Wilking, B. A., Lada, C. J., & Young, E. T. 1989, ApJ, 340, 823
Whitworth, A. P. & Ward-Thompson, D., 2001, ApJ, 547, 317
Young, C. H., Shirley, Y. L., Evans, N. J., II, Rawlings, J. M. C., 2003, ApJSS, 145, 111